Force Balance at the Magnetopause Determined with MMS: Application to Flux Transfer Events

C. Zhao[1], C. T. Russell[1], R. J. Strangeway[1], S. M. Petrinec[2], W. R. Paterson[3], M. Zhou[4], B. J. Anderson[5], W. Baumjohann[6], K. R. Bromund[3], M. Chutter[7], D. Fischer[6], G. Le[3], R. Nakamura[6], F. Plaschke[6], J. A. Slavin[8], R. Torbert[7] and H. Y. Wei[1]

[1] Department of Earth, Planetary and Space Sciences, University of California, Los Angeles, Los Angeles, CA, USA

[2] Lockheed Martin ATC, Palo Alto, California, USA

[3] NASA Goddard Space Flight Center, Greenbelt, Maryland, USA

[4] Department of Physics and Astronomy, University of California, Los Angeles, CA, USA

[5] Applied Physics Laboratory, The John Hopkins University, Laurel, MD, USA

[6] Space Research Institute, Austrian Academy of Sciences, Graz, Austria

[7] University of New Hampshire, Durham, NH, USA;

[8] University of Michigan, Ann Arbor, USA

Corresponding author: Cong Zhao (czhao@igpp.ucla.edu)

Key Points:

- Demonstrates flux transfer events are not necessarily force-free
- Finds that in non-force-free flux transfer events, the magnetic force is balanced by the ion pressure gradient force; the electron pressure gradient can be ignored
- Minimum variance analysis on the magnetic pressure gradient force gives the best estimate of the axial direction of flux ropes

This is the author manuscript accepted for publication and has undergone full peer review but has not been through the copyediting, typesetting, pagination and proofreading process, which may lead to differences between this version and the Version of Record. Please cite this article as doi: 10.1002/2016GL071568

Abstract

The Magnetospheric Multiscale mission (MMS) consists of four identical spacecraft forming a closely separated (≤ 10 km) and nearly regular tetrahedron. This configuration enables the decoupling of spatial and temporal variations and allows the calculation of the spatial gradients of plasma and electromagnetic field quantities. We make full use of the well cross-calibrated MMS magnetometer and fast plasma instruments measurements to calculate both the magnetic and plasma forces in flux transfer events (FTEs), and evaluate the relative contributions of different forces to the magnetopause momentum variation. This analysis demonstrates that some but not all FTEs, consistent with previous studies, are indeed force-free structures in which the magnetic pressure force balances the magnetic curvature force. Furthermore, we contrast these events with FTE events that have non-force-free signatures.

1 Introduction

Flux transfer events (FTEs) couple solar wind mass, momentum and energy to the magnetosphere through their magnetic connection between the magnetosheath plasma and the magnetospheric plasma. They are characterized by a unipolar magnetic field enhancement along the axial direction of the structure, and a transient bipolar magnetic field signature in the direction normal to the structure [Russell and Elphic, 1978]. **There are also some FTEs with a decrease of magnetic field strength in the center, additional to the typical unipolar magnetic field magnitude structure. This type of FTE is referred to as the crater FTE [Labelle et al., 1987; Farrugia et al., 1988].** The physical interpretation of the observed FTE phenomena is still subject to debate. The prevailing model of FTE structures is that of a magnetic flux rope [Elphic, 1990]. Other concepts for explaining these structures, like magnetopause waves [Sibeck, 1990], have proven to be inconsistent with the observations. Many attempts have been made to fit the observational FTE data to a parameterized flux rope model, some of them are based on the Lundquist [1950] force-free with circular cross-section flux rope model by, e.g. [Hasegawa et al., 2007; Scholer, 1995; Zhang et al., 2008], while others used the assumption that the flux rope is not magnetically force-free but still in force balance with the magnetic field and plasma pressures [Elphic and Russell, 1983; **Farrugia et al., 2016**]. The four MMS spacecraft with their close separation and inter-calibrated plasma and field instruments allow these hypotheses to be tested.

The NASA Magnetospheric Multiscale (MMS) Mission consists of four identical spacecraft, which form a nearly regular tetrahedron [Burch et al., 2016]. The separation of the spacecraft can be as close as 10km at the apogee during Phase 1a of the prime mission, with a separation knowledge of 10m. The magnetic field, electric field and plasma instruments onboard each spacecraft are identical and cross-calibrated. In the region of interest (greater than 9 Earth radii [Re] away from the Earth) the Fast Plasma Instruments (FPI) onboard the satellites operate at an unprecedented rapid cadence. In burst mode, the temporal resolution is a sample every

150ms for ions and 30ms for electrons, which is comparable to but longer than the 7.8ms burst-mode magnetic field data. These features facilitate the joint analysis of plasma and fields measurements to definitely and quantitatively answer physical questions related to the magnetic reconnection process by examining the variations of the directly measured physical quantities.

In this paper, we first briefly describe the data and methodology used to perform the pressure and curvature forces calculation. We then analyze four separate FTE events and present evidence that there are different types of FTEs.

2 Data and methodology

The data used in this paper are the magnetic field measurements from the fluxgate magnetometer (FGM) [Russell et al., 2016] and the plasma measurements from the Fast Plasma Instrument (FPI) [Pollock et al., 2016], which are onboard each of the four Magnetospheric Multiscale (MMS) spacecraft [Burch et al., 2016]. The data is collected at slightly different times from the instruments on the four spacecraft, so all data are interpolated to the time stamp of the magnetic field measurement of MMS1 for the cross-spacecraft and cross-instrument calculations. The times associated with the magnetometer measurements are also assigned to the center of each sample interval. However, the time stamp of the telemetered FPI data is associated with the beginning of each sample interval. In order to work on a common time descriptor between instrument data sets, we therefore assign a time to the FPI data that is shifted by half of its sample period. Thus the two data products are consistent with each other, and are centered on the same time.

The physical foundation of our discussion is based on the magneto-hydro-dynamic (MHD) momentum equation, given by Eq.1, while Eq.2 and Eq.3 give the parallel and perpendicular components of Eq.1.

Elphic et al. [1980] suggested that some flux ropes are force-free structures with current only along the field direction, such that both of the two terms $\boldsymbol{j} \times \vec{\boldsymbol{B}}$ and $\nabla \cdot \boldsymbol{P}$ in the right hand side of Eq. 1 are equal to zero.

$$\rho \frac{D\boldsymbol{u}}{Dt} = \boldsymbol{j} \times \boldsymbol{B} - \nabla \cdot \boldsymbol{P} \quad (1)$$

$$\rho \frac{D\boldsymbol{u}}{Dt}|_{\parallel} = -\boldsymbol{b}\,(\boldsymbol{b} \cdot \nabla P_{\parallel}) + \frac{(P_{\parallel} - P_{\perp})}{2 * P_m}(\boldsymbol{b} \cdot \nabla P_m)\boldsymbol{b} \quad (2)$$

$$\rho \frac{D\boldsymbol{u}}{Dt}|_{\perp} = (-\nabla_{\perp} P_m) + (-\nabla_{\perp} P_{i\perp}) + (-\nabla_{\perp} P_{e\perp}) + (2P_m + (P_{i\perp} - P_{i\parallel}) + (P_{e\perp} - P_{e\parallel}))\boldsymbol{\kappa}_c \quad (3)$$

where $P_m = \frac{B^2}{2\mu}$ is the magnetic pressure and $\boldsymbol{\kappa}_c = (\boldsymbol{b} \cdot \nabla)\boldsymbol{b}$ is the curvature of the magnetic field.

The terms on the right hand side of Eq. 3 are the perpendicular gradient of magnetic pressure, the perpendicular gradient of ion perpendicular pressure, the perpendicular gradient of electron perpendicular pressure, the magnetic curvature force associated with the magnetic pressure and the magnetic curvature force associated with the ion and electron anisotropy respectively.

The numerical method related to the calculation of the different terms in Eq. 3 is the calculation of the gradient of a vector or scalar field [Harvey, 1998]. Assume $\mathbf{k} = \nabla \mathrm{m}$ is the gradient tensor of the scalar field m. Define the function S to be the summation of the residue of the 1st order Taylor expansion of m

$$S = \sum_{\alpha=1}^{N} \sum_{\beta=1}^{N} |[\mathbf{k} \cdot (\boldsymbol{r}_\alpha - \boldsymbol{r}_\beta) - (m_\alpha - m_\beta)]|^2 \qquad (4)$$

$\boldsymbol{r}_\alpha$ in Eq.4 is the location of spacecraft α in mesocenter frame, where the mesocenter is defined as the average location of the four spacecraft.

In order to obtain the best estimation of $\mathbf{k} = \nabla m$, we need $\frac{\delta S}{\delta k_{ij}} = 0$. By solving this equation, we obtain:

$$k_j = \frac{1}{N^2}[\sum_{\alpha \neq \beta}(m_\alpha - m_\beta)(r_{\alpha k} - r_{\beta k})]R_{kj}^{-1} \qquad (5)$$

where $R_{ij} \equiv \frac{1}{N}\sum_{\alpha=1}^{N} r_{\alpha i} r_{\alpha j}$

Similarly, the gradient $\mathbf{k}$ of a vector $\boldsymbol{b}$ is $k_{ij} = \frac{1}{N^2}[\sum_{\alpha \neq \beta}(b_{\alpha i} - b_{\beta i})(r_{\alpha k} - r_{\beta k})]R_{kj}^{-1}$ (6).

For each flux transfer event, the physical quantities are examined in the local FTE-LMN coordinates as illustrated schematically in Figure 1. Because both the current and the magnetic field component along the direction of rope axis are not constant, the minimum variance analysis on them would not result in an accurate rope axial direction. However, based on the assumption that the flux rope pressure profile is uniform along the axial direction, the pressure gradient acts only perpendicular to the rope axis (green vectors in Figure 1). Thus minimum variance analysis on the magnetic pressure gradient will lead to an accurate rope axial direction, thereby we define this direction as L direction. When the spacecraft is at its closet encounter to the FTE, i.e. when the magnetic field magnitude maximizes in the time series, the field can only have two

components (as shown in Figure 1b), one along rope axis and the other along the spacecraft trajectory projected in M-N plane, which means $\boldsymbol{B}_{max}=\boldsymbol{B}_M+\boldsymbol{B}_{\mathrm{L}}$. So the N direction can be obtained through $\mathbf{N} = (\boldsymbol{B}_{max}\times \mathbf{L})/|\boldsymbol{B}_{max}\times \mathbf{L}|$. Last, **M** completes the right hand coordinate system.

3 Force free and non-force-free flux transfer event cases

Figure 2a shows an overview of the first event on Oct 16th 2015. This appears to be a partial magnetopause crossing. The MMS fleet went from the magnetosphere into the magnetopause boundary layer at around 13:04:15 UT and went back into the magnetosphere at around 13:04:52 UT, and there is no evidence of pure magnetosheath properties recorded by the MMS fleet. Two flux transfer events (FTE), or flux ropes, are found in the middle of this partial magnetopause crossing. They have been interpreted to be two adjacent islands formed by magnetic reconnection [*Eastwood et al.*, 2016]. Figure 2b is an overview of another FTE event on Dec 14th 2015. The MMS spacecraft left the magnetopause at around 00:58:00 UT and went partially through the magnetopause and back into the magnetosphere at around 00:59:40 UT. The flux rope is embedded in the magnetopause layer and encountered the MMS fleet from 00:58:57 UT to 00:59:01 UT. The last panels in Figure 2a and Figure 2b contain the current calculated from the curlometer. It is clearly demonstrated that the current in the magnetopause is flowing in both the parallel and perpendicular directions with comparable strengths, while the current inside the FTEs mainly flows along the magnetic field line. The expansion in Figure 3a, 3b and 3c shows the detailed structure of these three FTEs in the local FTE LMN coordinates. In each plot in Figure 3, lines *a* and *d* denote the start and end of each FTE event respectively, while line *b* denote the time of maximum magnetic field strength inside the FTE.

In Figures 3a, 3b and 3c, the magnetic field profiles exhibit bipolar structure in the N component and a unipolar structure in the L component, which is strong evidence for encountering a flux transfer event [*Russell and Elphic*, 1979]. The second event is nearly symmetric with respect to line b_2, the time when the magnetic field magnitude reaches its maximum. The third event, on the other hand, is asymmetric around the maximum of |B|. The first event exhibits the signature of a crater FTE. This topological difference in magnetic profile is evidence that an asymmetry could exist in the FTE, i.e. it may not be a perfectly circular flux rope. Using the multi-spacecraft timing method, the velocity and direction (in LMN coordinates) of the three events are measured to be 260km/s [0.44, -0.86, 0.27], 260km/s [0.70, -0.67, -0.22] and 180 km/s [0.70 -0.71, 0.08] respectively. The cross section diameter of the three FTEs are 950km, 1050km and 900km respectively.

The 6th panel of each event shows the parallel and perpendicular current from the curlometer calculation. The parallel component dominates the current flowing through the flux transfer event in all three cases with a magnitude of about 500 nA/m^2. The current drops to around zero in the middle of the three FTEs (marked by line c_1, c_2 and c_3 respectively), but surprisingly not coincident with the maximum of magnetic field strength. The perpendicular current is nearly an order of magnitude smaller than the parallel current throughout FTE1 and FTE2, which reveals the near force-free property of the flux transfer events, while the magnitude of the perpendicular current is comparable to the parallel current in part of FTE3 (between line d3 and e3). However, there is no absolute threshold of current strength to determine whether the structure is magnetic force-free or not. A plausible way to classify force-free and non-force-free structures would be to find out the relative dominant terms in the momentum equation to check whether or not they are purely magnetic terms or not. A FTE where purely magnetic terms determine the momentum balance would be a force-free structure.

This property is examined in more detail in the remaining panels in Figure 3. The last four panels of each displayed event are the three components as well as the magnitude of the magnetic pressure force components (in light red), the magnetic curvature force (in dark green) component of the jxB force, the ion pressure gradient (in light blue), as well as the total force exerted on the FTEs (in black). These force analyses definitively show that the magnetic curvature force in FTE1 and FTE2 is always opposite the magnetic pressure force and result in much smaller total magnetic force (i.e. jxB force). But the magnetic pressure and curvature force magnitudes vary considerably in these three events. The force magnitudes are 2 pPa/km and 8pPa/km respectively. In each individual event, the force profile also demonstrates apparent asymmetry. For example, in FTE2, the normal component of the force is much larger before the maximum of the magnetic field strength intensity than thereafter.

Although FTE3 shares a similar feature as those of FTE1 and FTE2 (the magnetic curvature force also opposes the magnetic pressure force), a significant difference is that the magnetic curvature force is much smaller than magnetic pressure force (especially in the normal direction) and results in a non-vanishing magnetic force in case FTE3. Also shown in the second last panel of Figure 3c, the non-zero jxB force is balanced by the ion pressure gradient force. So FTE3 is not a force-free structure but involves force balance between non-zero magnetic and plasma forces.

In order to prove that the non-force-free FTE3 is not unique, we also present a fourth FTE (FTE4) in Figure 4a. The velocity of FTE4 is close to 146km/s, which leads to a much larger diameter of 4700km. The current in FTE4 is concentrated in the very central part of this FTE. The total magnetic force has two very large (~30pPa/km) peaks in the center of this FTE. This force is also balanced by the ion pressure gradient force, similar to FTE3. In Figure 4b, the 5 second interval (between b4 and e4 in Figure 4a) in which the magnetic pressure force is peaked is presented, and shows evidence that the magnetic force is balanced by the ion pressure gradient force in the “crater” part of FTE3. In FTE4, the parallel current changed from along the

magnetic field to anti-parallel to the magnetic field marked by line f4 and g4, right after the ion pressure gradient and magnetic pressure gradients reach their maxima. This anti-parallel current untwists the field line, providing evidence that the physical process inside the crater is very dynamic.

Also plotted in the last four panels of Figure 4b is the electron pressure gradient force (in dark red), the curvature force due to the ion anisotropy (in light green) and the curvature force due to the electron anisotropy (in dark blue). As shown in the figure, these three components of Eq.3 prove to be around zero, so they do not contribute significantly much to the momentum variation of the FTEs compared to the ion pressure gradient force. This is expected because the temperature of electrons is usually much smaller than the ion temperature. This is also the case with the other 3 FTEs, although not explicitly shown in their force analysis plots.

4 Conclusions

The diagnostic capability of the MMS mission, with four identical satellites forming a closely separated tetrahedron with high resolution plasma and magnetic field measurements, was fully exploited in this study to perform a quantitative analysis of the forces associated with the four flux transfer events. First, the force analysis procedure was used to determine the axial direction of the flux transfer event by estimating the minimum variation direction of the magnetic pressure force, because the flux rope does not push along its axis. The force analysis provides much more information than the current analysis by itself. Through this powerful tool enabled by the MMS mission, we demonstrate that there are force-free flux transfer event cases as predicted by *Lundquist* [1950] in which the magnetic pressure force is balanced by the magnetic curvature force. However, there are also FTEs in which the magnetic curvature force is not sufficient to balance the magnetic pressure force. Therefore, the plasma force, and especially the ion pressure force must be taken into account in the FTE force balance, while the electron contribution is usually small and can be ignored. To study the dynamics of FTE, both the ion and magnetic structure must be examined.

Acknowledgments

The work at UCLA was supported through subcontract 06-001 with the University of New Hampshire.

References

Burch, J. L., et al. (2016), Electron-scale measurements of magnetic reconnection in space,

Science, *352*(6290), aaf2939, doi:10.1126/science.aaf2939.

Eastwood, J. P., et al. (2016), Ion-scale secondary flux ropes generated by magnetopause reconnection as resolved by MMS, *Geophysical Research Letters*, *43*(10), 4716-4724, doi:10.1002/2016gl068747.

Elphic, R. C. (1990), Observations of Flux Transfer Events: Are FTEs Flux Ropes, Islands, or Surface Waves?, in *Geoph Monog Series*, edited, pp. 455-471, American Geophysical Union, doi:10.1029/GM058p0455.

Elphic, R. C., and C. T. Russell (1983), Magnetic-Flux Ropes in the Venus Ionosphere - Observations and Models, *J Geophys Res-Space*, *88*(Na1), 58-72, doi:DOI 10.1029/JA088iA01p00058.

Elphic, R. C., C. T. Russell, J. A. Slavin, L. H. Brace, and A. F. Nagy (1980), The Location of the Dayside Ionopause of Venus - Pioneer Venus Orbiter Magnetometer Observations, *Geophysical Research Letters*, *7*(8), 561-564, doi:DOI 10.1029/GL007i008p00561.

Farrugia, C. J., R. P. Rijnbeek, M. A. Saunders, D. J. Southwood, D. J. Rodgers, M. F. Smith, C. P. Chaloner, D. S. Hall, P. J. Christiansen, and L. J. C. Woolliscroft (1988), A multi-instrument study of flux transfer event structure, *Journal of Geophysical Research*, *93*(A12), 14465, doi:10.1029/JA093iA12p14465.

Farrugia, C. J., et al. (2016), Magnetospheric Multiscale Mission observations and non-force free modeling of a flux transfer event immersed in a super-Alfvénic flow, *Geophys Res Lett*, *43*(12), 6070-6077, doi:10.1002/2016gl068758.

Harvey, C. C. (1998), Spatial Gradients and the Volumetric Tensor, Analysis Methods for Multi-Spacecraft Data, Edited by Paschmann, G. and Daly, P.W., *ISSI Scientific Report Series*, *1*, 307-322.

Hasegawa, H., R. Nakamura, M. Fujimoto, V. A. Sergeev, E. A. Lucek, H. Reme, and Y. Khotyaintsev (2007), Reconstruction of a bipolar magnetic signature in an earthward jet in the tail: Flux rope or 3D guide-field reconnection? *J Geophys Res-Space*, *112*(A11), Artn A11206, Doi:10.1029/2007ja012492.

Labelle, J., R. A. Treumann, G. Haerendel, O. H. Bauer, G. Paschmann, W. Baumjohann, H. Luhr, R. R. Anderson, H. C. Koons, and R. H. Holzworth (1987), Ampte Irm Observations of Waves Associated with Flux-Transfer Events in the Magnetosphere, *J Geophys Res-Space*, *92*(A6), 5827-5843, doi:DOI 10.1029/JA092iA06p05827.

Lundquist, S. (1950), Magneto-Hydrostatic Fields, *Ark Fys*, *2*(4), 361-365.

Pollock, C., et al. (2016), Fast Plasma Investigation for Magnetospheric Multiscale, *Space Sci Rev*, *199*(1-4), 331-406, doi:10.1007/s11214-016-0245-4.

Russell, C. T., et al. (2016), The Magnetospheric Multiscale Magnetometers, *Space Sci Rev*, *199*(1-4), 189-256, doi:10.1007/s11214-014-0057-3.

Russell, C. T., and R. C. Elphic (1978), ISEE-1 and ISEE-2 Observations of Flux-Transfer Events on Dayside Magnetopause, *Eos T Am Geophys Un*, *59*(12), 1162-1162.

Russell, C. T., and R. C. Elphic (1979), ISEE Observations of Flux-Transfer Events at the Dayside Magnetopause, *Geophys Res Lett*, *6*(1), 33-36, doi:Doi 10.1029/Gl006i001p00033.

Scholer, M. (1995), Models of Flux Transfer Events, in *Physics of the Magnetopause*, edited, pp. 235-245, American Geophysical Union, doi:10.1029/GM090p0235.

Sibeck, D. G. (1990), A Model for the Transient Magnetospheric Response to Sudden Solar-Wind Dynamic Pressure Variations, *J Geophys Res-Space*, *95*(A4), 3755-3771, doi:DOI 10.1029/JA095iA04p03755.

Zhang, H., K. K. Khurana, M. G. Kivelson, V. Angelopoulos, Z. Y. Pu, Q. G. Zong, J. Liu, and X. Z. Zhou (2008), Modeling a force-free flux transfer event probed by multiple Time History of Events and Macroscale Interactions during Substorms (THEMIS) spacecraft, *J Geophys Res-Space*, *113*(A1), doi:Artn A00c0510.1029/2008ja013451.

Figure Captions:

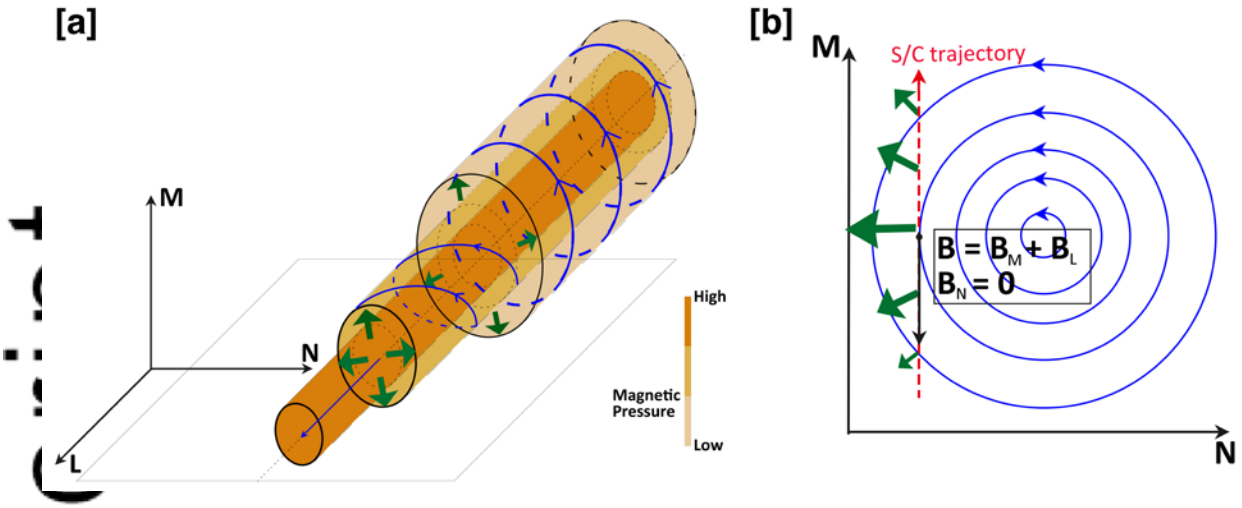

Figure 1 Schematic picture of: [a] the flux rope 3D structure, [b] the cross-section perpendicular to the axis of the flux rope. The blue arrows show the magnetic field line, green arrows point along the pressure gradient direction, while the red arrow is the spacecraft trajectory. Dark, medium and light yellow fill color illustrate the different pressure values.

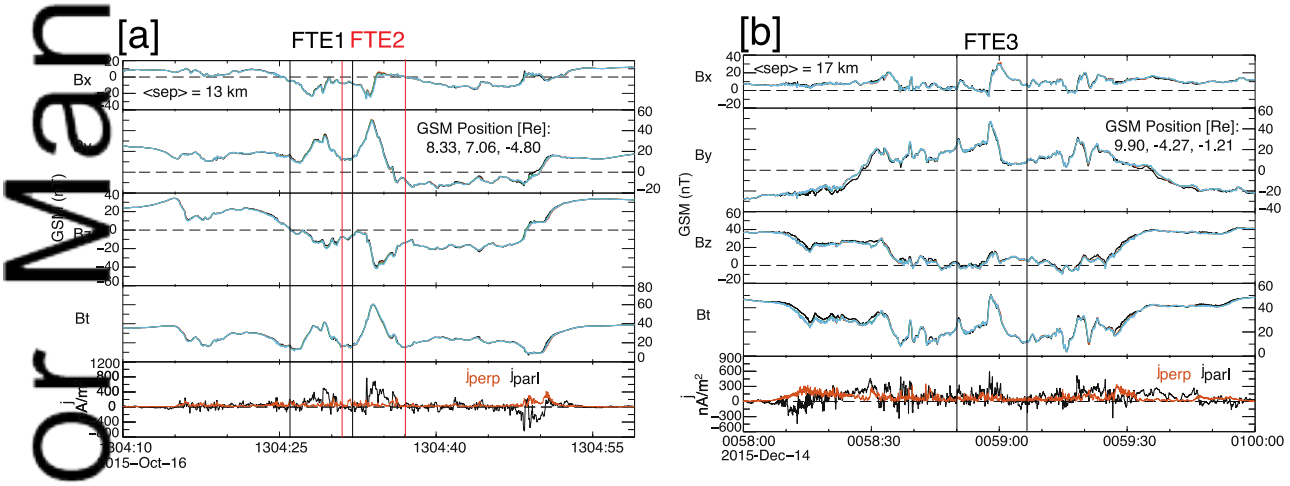

Figure 2 Overview of three flux transfer event embedded between two partial magnetopause crossing, [a] the magnetopause crossing on October 16, 2015 and two FTEs; [b] the magnetopause crossing on December 14, 2015 and one FTE contained within it. For both plots, the first four panels are the GSM X, Y, Z component and intensity of the magnetic field of the four MMS spacecraft in black (MMS1), light red (MMS2), light green (MMS3) and light blue (MMS4), respectively. The last panel shows the current from the curlometer, the black trace is the current parallel to the magnetic field and the light red trace is the perpendicular current

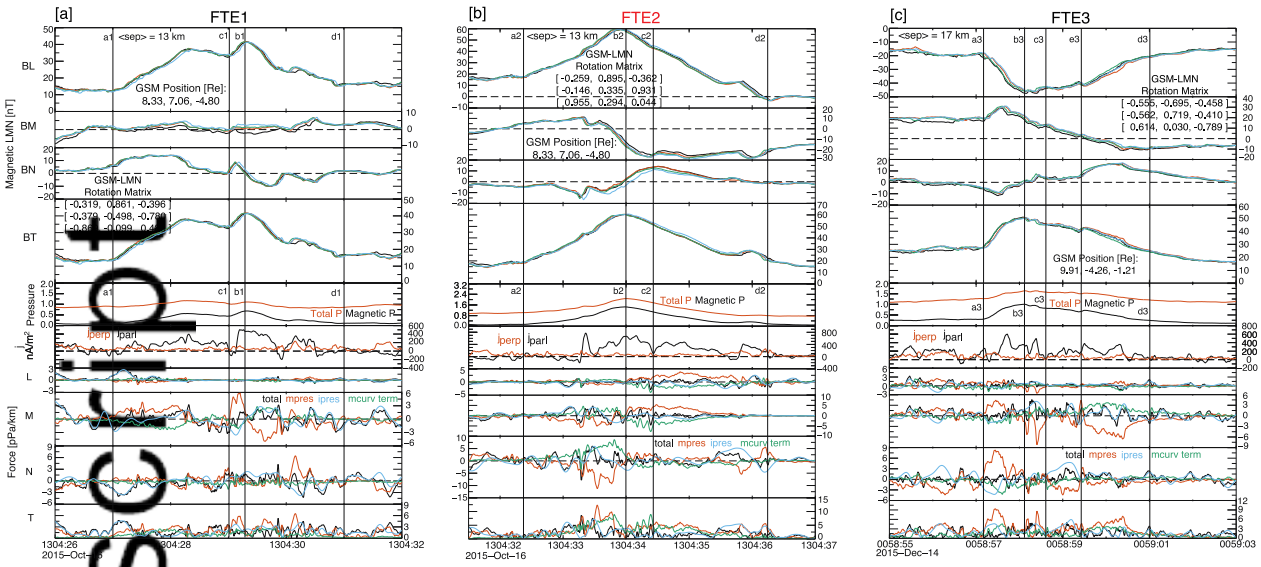

Figure 3. Three FTEs, the first four panels are the L, M, N component and intensity of the magnetic field for the four MMS spacecraft in black (MMS1), light red (MMS2), light green (MMS3) and light blue (MMS4), respectively. The fifth panel is the magnetic pressure in red and total pressure in black. The sixth panel is the current from the curlometer, the black trace is the current parallel to the magnetic field and the light red trace is the perpendicular current. The last four panels are the L, M, N direction and total of the force analysis, with the black being the summation of different force contribution, the light red being the magnetic pressure gradient force, the light blue being ion pressure gradient force and light green being the magnetic curvature force.

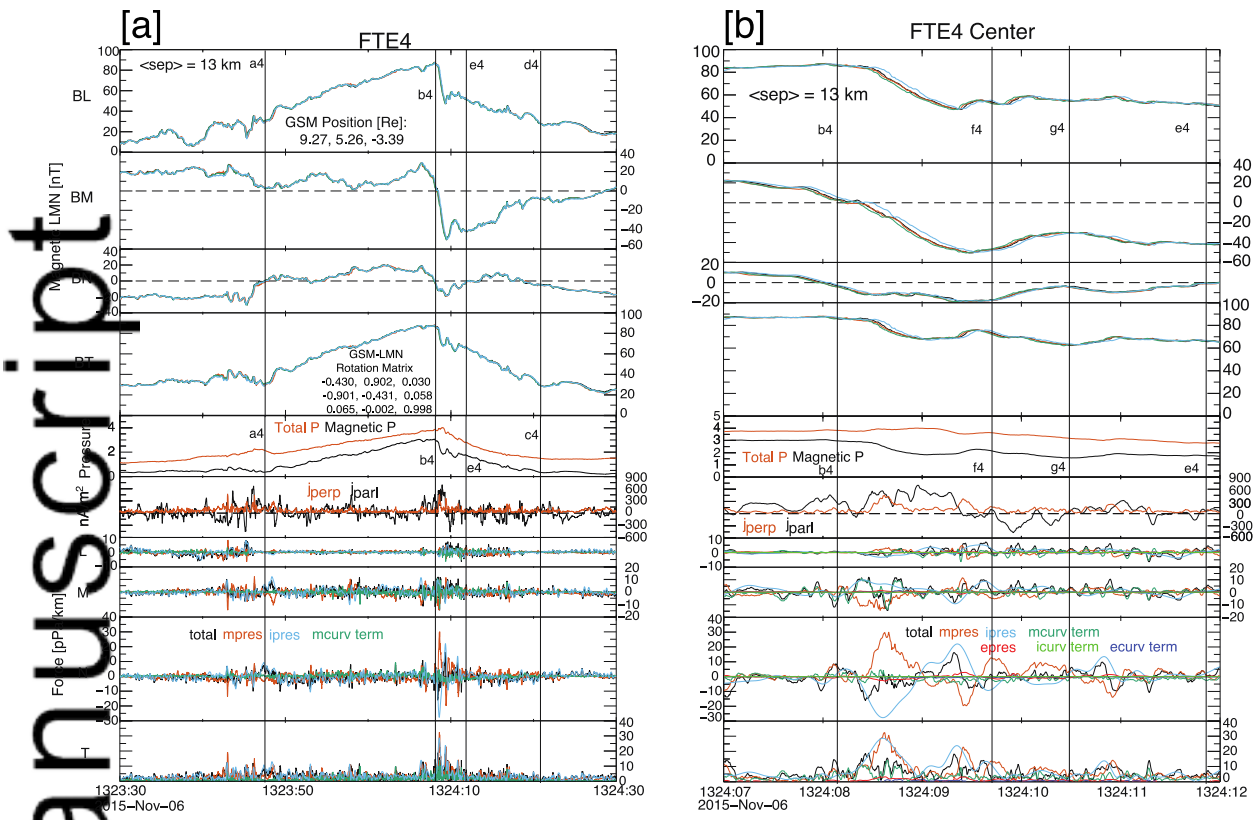

Figure 4. [a] The fourth FTE, which is non-force free and [b] the center part of this FTE, where large magnetic and plasma force exist. The plot format is the same as Figure 3.

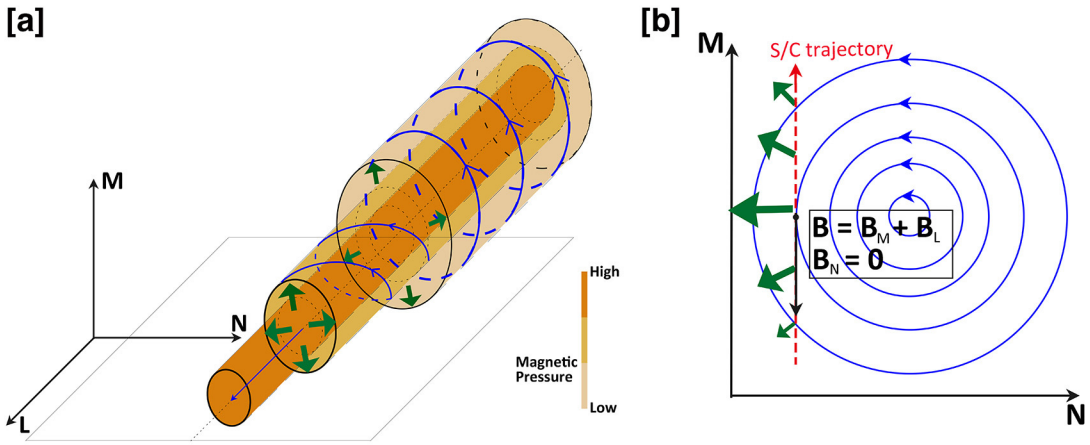

2016GL071568-f01-z-.jpg

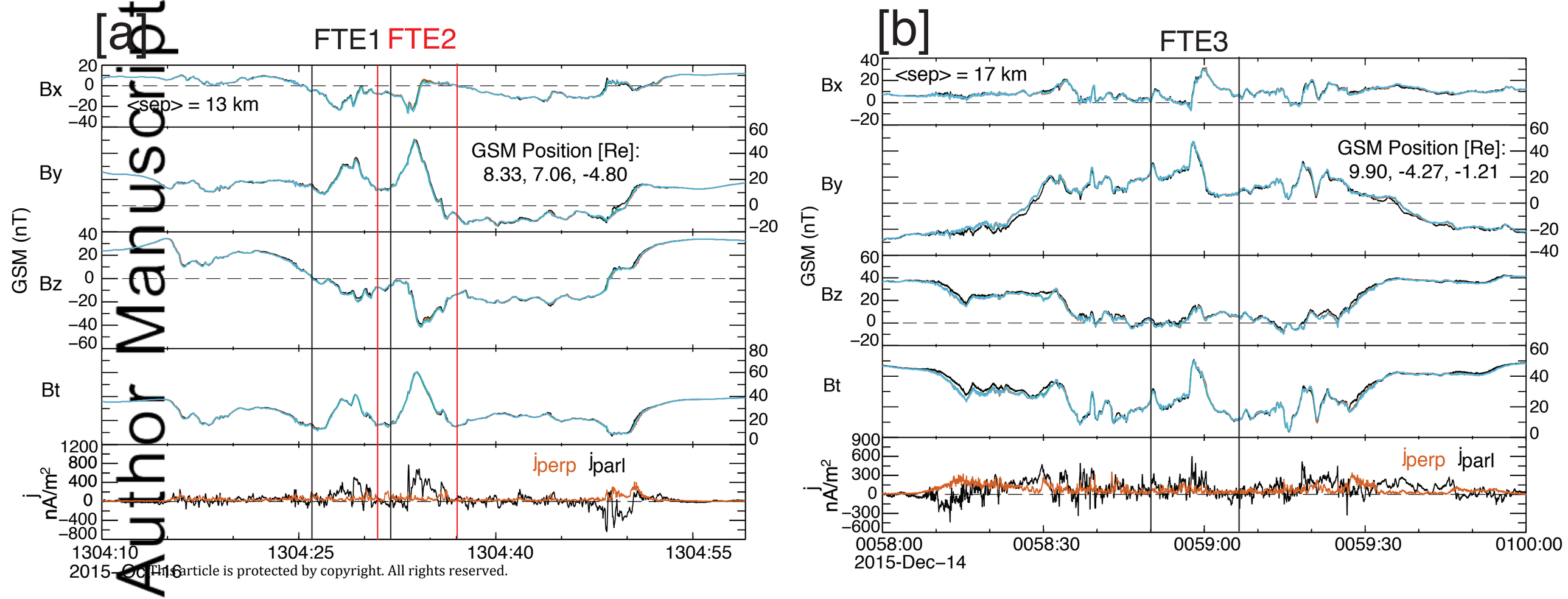

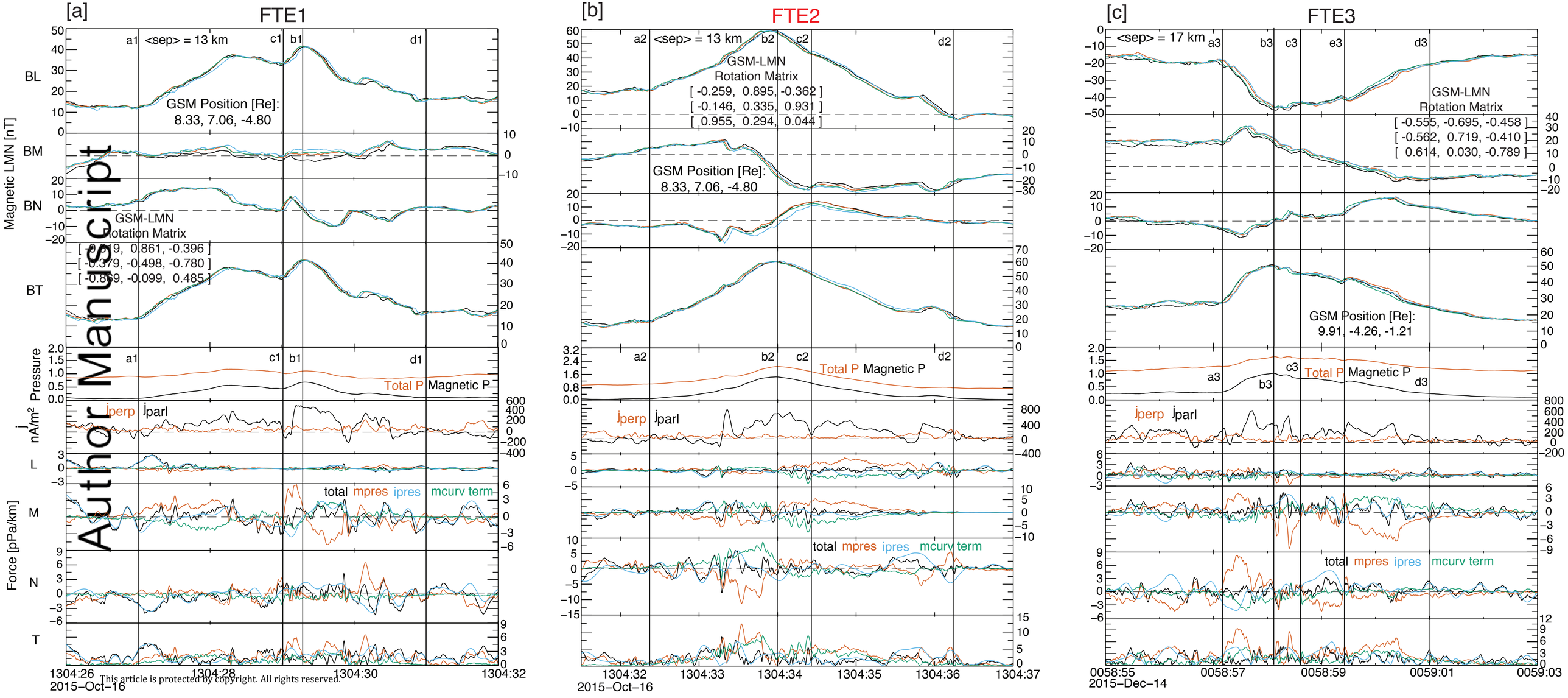

[a]

FTE4

<sep> = 13 km

a4 b4 e4 d4

GSM Position [Re]:
9.27, 5.26, -3.39

BL

BM

BN

BT

GSM-LMN
Rotation Matrix
-0.430, 0.902, 0.030
-0.901, -0.431, 0.058
0.065, -0.002, 0.998

Magnetic LMN [nT]

Pressure

a4 b4 e4 c4

Total P Magnetic P

j nA/m²

jperp jparl

L

M

N

T

total mpres ipres mcurv term

Force [pPa/km]

1323:30
2015–Nov–06

1323:50

1324:10

1324:30

[b]

FTE4 Center

<sep> = 13 km

b4 f4 g4 e4

Total P Magnetic P

jperp jparl

total mpres ipres mcurv term
epres icurv term ecurv term

1324:07
2015–Nov–06

1324:08

1324:09

1324:10

1324:11

1324:12